ACS APPLIED MATERIALS & INTERFACES

RESEARCH ARTICLE

www.acsami.org

Fluorescence Sensing of Zinc(II) Using Ordered Mesoporous Silica Material (MCM-41) Functionalized with *N*-(Quinolin-8-yl)-2-[3-(triethoxysilyl)propylamino]acetamide

Parul Pal,[†,‡] Shiva K. Rastogi,[*,†,§] Charlene M. Gibson,[§] D. Eric Aston,[⊥] A. Larry Branen,[§] and Thomas E. Bitterwolf

[†]Department of Chemistry, University of Idaho, Moscow, Idaho 83844-2343, United States

[§]Biosensors and Nanotechnology Applications Laboratory, University of Idaho, Coeur d'Alene, Idaho 83814-2277, United States

[⊥]Department of Chemical and Materials Engineering, University of Idaho, Moscow, Idaho 83844-1021, United States

Supporting Information

ABSTRACT: A novel fluorescent zinc sensor was designed and synthesized on ordered mesoporous silica material, MCM-41, with *N*-(quinolin-8-yl)-2-[3-(triethoxysilyl)propylamino]acetamide (QTEPA; **3**) using a simple one-step molecular self-assembly of the silane. The solution and solid samples were characterized using solid-state nuclear magnetic resonance, transmission electron microscopy, diffuse-reflectance infrared Fourier transform, and thermogravimetric analysis techniques. The QTEPA-modified MCM-41 (**4**) shows 3-fold fluorescence emission enhancement and about a 55 nm red shift upon addition of 1 μM Zn^{II} ions in a Tris-HCl (pH 7.22) aqueous buffer solution. The UV−vis absorption maximum is at 330 ± 5 nm, and the fluorescence emission maximum wavelength is at 468 nm, with an increase in quantum yield from 0.032 to 0.106 under the same conditions. The presence of other metal ions has no observable effect on the sensitivity and selectivity of **4**. This system selectively detects Zn^{II} ions with submicromolar detection to a limit of 0.1 μM. The MCM-41-based systems have the advantage that they can be employed in aqueous solutions without any aggregation.

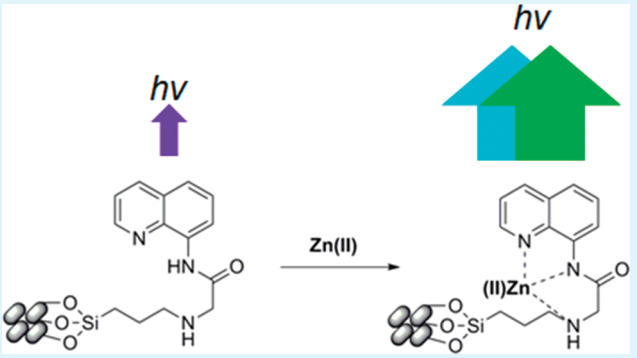

KEYWORDS: MCM-41, quinoline, zinc sensor, Tris-HCl buffer, DRIFT, fluorescence detection

1. INTRODUCTION

Fluorescence detection of divalent cations is the most common method employed for biological sensing of metals, especially calcium and magnesium.[1] Designing sensors to be highly selective and sensitive toward a particular analyte is a challenge. In addition, the effects of interfering ions should also be taken into consideration. This becomes even more difficult when the analyte, such as zinc, is present at much lower concentration compared to other common metals in biological systems.

Biological sensing of zinc has come into prominence in the past 2 decades.[2−5] Existing primarily as zinc(II) in biological systems, it is the second most abundant transition metal only next to iron.[6,7] In the human body, the concentration of zinc(II) varies in different physiological environments and ranges from 12 μM in intracellular serum to about 0.1−0.5 mM in brain and nerve tissues.[8] Most of the zinc is sequestered by proteins and is responsible for multiple physiological roles such as gene transcription, metalloenzyme regulation, and neural signal transmission.[6,8−11] Severe neurological diseases such as Alzheimer's and Parkinson's are reported to be closely related to disorders in zinc metabolism.[8−11]

The $3d^{10}4s^0$ electronic configuration of zinc(II) renders it spectroscopically silent toward conventional optical methods of detection, making fluorescence the most efficient way of detecting zinc in biological systems.[6,8,10] Detecting zinc in low concentrations in vivo has attracted several researchers to develop fluorescence chemosensors or biosensors, most of which involve signal amplification upon identifying (or binding) the metal in question. Typical designs for such a sensor include a recognition moiety, usually a chelating group, responsible for the selectivity of the analyte. The recognition moiety is connected, via a spacer or not, to one or more photoactive units that generate the fluorescence signal.[12−14]

Some of the early sensors for fluorescence detection of zinc(II) were based on derivatives of quinoline such as TSQ,[15] Zinquin,[16−18] and TFLZn.[19] These arylsulfonamides of quinolines incorporate macrocyclic zinc(II) binding units but were,

Received: September 25, 2010
Accepted: December 8, 2010
Published: January 18, 2011

Scheme 1[a]

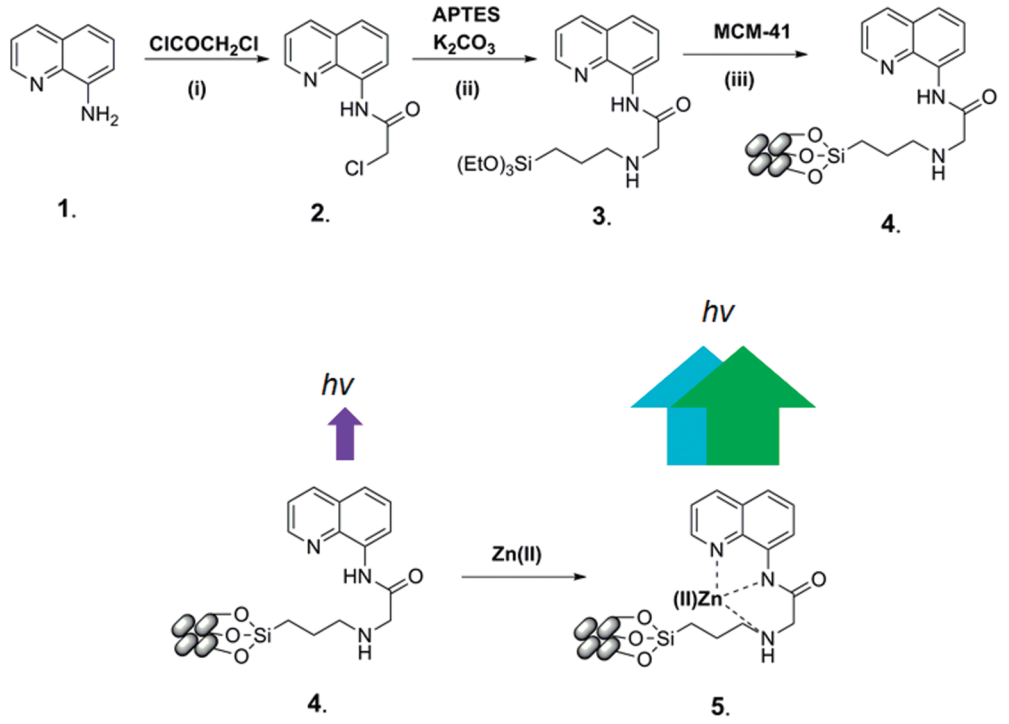

[a] (i) 8-Aminoquinoline (8 mmol); chloroacetyl chloride (9.6 mmol); pyridine (11.2 mmol); CH_2Cl_2 (50 mL); 0 °C to rt, 2 h. (ii) APTES (2.5 mmol); anhydrous K_2CO_3 (3.41 mmol) and **2** (2.27 mmol), dry CH_3CN (40 mL); rt to Δ for 4 h. (iii) MCM-41 (100 mg); anhydrous toluene (40 mL); 0.015 mmol of **3**, Δ for 8 h. The addition of Zn^{II} ions in a suspension of **4** results in enhancement in the fluorescence intensities of **5**.

however, used only for fluorescence imaging upon zinc(II) binding. Nonetheless, supramolecular systems of quinolines, especially 8-aminoquinolines, offer an attractive option for developing highly selective zinc(II) sensors even over other possible competing cations.[8]

The operation of these sensors is mostly based on signal amplification as a result of zinc(II) binding. This phenomenon, also termed chelation enhanced fluorescence, operates by the mechanism of photoinduced electron transfer (PET).[6,22−25] In the case of 8-aminoquinoline, the lone pair of electrons of the 8-amino residue are transferred to the π system of fluorophore upon excitation, which, in turn, results in suppression of the fluorescence intensity. The involvement of the lone pair of electrons in binding of the metal ions inhibits the PET process, resulting in an increase of the fluorescence intensities. This phenomenon is preferred because it is visually perceptive. This principle is applied in most of the zinc(II) sensors, a process that is well studied and explained in several reviews.[6,12−14,26−29]

The reported sensors for zinc(II) based on 8-aminoquinoline, however, suffer from low water solubility.[30] In addition, the "naked" sensor may encounter interference by proteins or membrane binding.[6,31] These problems can, however, be overcome by the use of highly sophisticated hosts containing multiple binding sites, which should also increase the analyte−receptor interaction.[32] Materials chemistry has made advances in developing organic or inorganic frameworks that can mimic certain features of biological structures such as membranes, ion channels, and their selection properties or surface activities.[32] The rigid but porous nature of these materials such as ordered mesoporous silica materials, MCM-41, allows inner functionalization with the desired organic moiety.[33−36]

First synthesized in the early 1990s by Mobil Corp.,[37,38] the MCM-41 class of materials has been widely used as supports for catalysis, as molecular sieves, for chemical and biological sensing, for specific adsorption, and in optical diagnostic applications. The high surface area and the availability of surface silanols allow for covalent grafting of the organic functionality at high density,[33−36] which, in turn, translates to a higher response rate of the final solid.[32]

The porous silica system may also provide protection of the signaling molecule.[39] Specifically for optical applications, these materials possess the advantage of having optical transparency in the visible region and guarantee fastness toward UV radiation.[40] Consequently, several groups have successfully developed sensors such as those for detecting ATP,[41,42] SO_2,[43] fluoride,[39] and copper(II);[44] but none so far have been reported, to the best of our knowledge, for detecting zinc(II).

We present here a sensor design based on high-surface-area MCM-41 to realize a selective and sensitive detection of zinc(II) in suspension. Covalent modification of the surface is achieved with 8-aminoquinoline via (3-aminopropyl)triethoxysilane and chloroacetyl chloride as a linker (Scheme 1). The fluorophore attached on MCM-41 **4** is a tridentate chelating moiety, with maximum UV−vis absorbance at 330 ± 5 nm and a fluorescence emission maximum at 468 nm upon zinc(II) binding. The detection limit for zinc(II) achieved by our system is 0.1 μM, lower than previously reported for similar systems[30,45,46] and can be used at physiological pH (7.2−7.4).

2. EXPERIMENTAL SECTION

2.1. Materials. MCM-41 [a Brunauer−Emmett−Teller (BET) surface area of 880 m^2/g and an average pore size of 37 Å) was provided

by the Pacific Northwest National Laboratory. All of the chemicals and reagents were purchased from Sigma-Aldrich, St. Louis, MO, and Fisher Scientific, Pittsburgh, PA, and used without further purification. The solvents used for the reactions were stored in bottles with appropriate drying agents, and freshly distilled before use. NaCl, KCl, $CaCl_2$, $MgCl_2$, $CrCl_2$, $MnCl_2$, $FeCl_2$, $CoCl_2$, $NiCl_2$, $CuSO_4 \cdot 5H_2O$, $ZnNO_3 \cdot 6H_2O$, $CdCl_2$, $HgCl_2$, $PbNO_3$, and $ThNO_3$ were of analytical grade. Doubly distilled deionized water (DIW) was used for all experiments, and solution NMR was carried out in dimethyl sulfoxide (DMSO)-d_6, purchased from Sigma-Aldrich.

2.2. Instruments. ^{1}H and ^{13}C NMR on solution samples and ^{29}Si and ^{13}C NMR on solid samples were measured on a Bruker Avance 500 MHz spectrometer. All of the solid-state NMR spectra were measured using a 4 mm (o.d.) zirconia rotor with a Kel-F cap. Solid-state ^{29}Si NMR was performed under magic-angle-spinning (MAS) conditions with a pulse delay of 1 min and a spinning rate of 12 kHz. For solid-state ^{13}C NMR, cross-polarization (CP), along with MAS, was used with a pulse delay of 2 s and a spinning rate of 7−8 Hz. Chemical shifts for MAS ^{29}Si NMR were referenced to the external standard TTMS. All solid and solution NMR experiments were performed at room temperature.

Solid-state IR using diffuse-reflectance infrared Fourier transform (DRIFT) spectroscopy was performed using a Nicolet Magna-IR(R) ESPTM System 760 with a DTGS detector and IR-grade KBr as the internal standard. Transmission electron microscopy (TEM) images were obtained on a JEOL 1200 EX II transmission electron microscope equipped with a LaB6 gun with 0.5 nm resolution. Thermogravimetric analysis (TGA) was carried out on a TGA Q50 V6.7 instrument. All TGA experiments were carried out under a nitrogen atmosphere at a heating rate of 10 °C/min from 22 to 800 °C. An exeter CE440 elemental analyzer was used to determine the C, H, and N content. Fluorescence and absorption spectra were acquired with a Jobin-Yvon-Horiba spectrometer and a Shimadzu UV−vis spectrophotometer, respectively.

2.3. Synthesis of *N*-(Quinoline-8-yl)-2-[3-(triethoxysilyl)-propylamino]acetamide (QTEPA; 3). The precursor, 8-[(chloroacetyl)amino]quinoline (**2**), was prepared by the literature method. The silane, **3**, was prepared by reacting 2.5 mmol of (3-aminopropyl)triethoxysilane (APTES) with 2.27 mmol of **2** in the presence of anhydrous K_2CO_3 (4.305 mmol) in 40.0 mL of dry acetonitrile. The reaction mixture was refluxed for 4.0 h, filtered through a sintered funnel, and allowed to stand overnight at room temperature (rt). The solution was filtered again to remove white residue, and upon removal of the solvent, yielded yellow oil (72%). This was used for the next step without further purification. ^{1}H NMR (500.13 MHz, DMSO-d_6): δ 0.71 (t, J = 8.44 Hz, 2H, $SiCH_2^*CH_2CH_2N$), 1.07 (t, J = 7.00 Hz, 9H, $Si(OCH_2CH_3^*)_3$), 1.57 (tt, J = 8.40 and 6.70 Hz, 2H, $SiCH_2CH_2^*CH_2N$), 2.60 (t, J = 6.70 Hz, 2H, $SiCH_2CH_2CH_2^*N$), 3.35 (s, 2H, $(CO)CH_2^*NH$), 3.67 (q, J = 7.00 Hz, 6H, $Si(OCH_2^*CH_3)_3$); quinoline H, δ 7.55−7.66 (m, 3H), 8.40 (dd, 1H), 8.72 (dd, 1H), 8.88 (dd, 1H), 11.50 (s, 1H, $(CO)CH_2NH^*$). ^{13}C NMR (125.76 MHz, DMSO-d_6): δ 7.44 ($SiC^*H_2CH_2CH_2N$), 18.25 ($Si(OCH_2C^*H_3)_3$), 22.94 ($SiCH_2C^*H_2CH_2N$), 52.52 and 53.34 ($SiCH_2CH_2C^*H_2N$ and $(CO)C^*H_2NH$), 57.53 ($Si(OC^*H_2CH_3)_3$); quinoline C, δ 115.20, 121.48, 121.98, 126.96, 127.81, 134.15, 136.42, 138.04, 148.78, 170.89 (CO). ^{29}Si NMR (99.36 MHz, DMSO-d_6): δ −44.0.

2.4. Functionalization of MCM-41 with 3. In a round-bottomed flask, 100.0 mg of MCM-41 was suspended in 40.0 mL of anhydrous toluene. To optimize the functionalization process, hydration of the surface was carried out with approximately two monolayers of DIW. The stoichiometry was based on the measured surface area (880 m^2/g), and it was assumed that there are 5×10^{18} molecules/m^2 in fully dense monolayer coverage.[47,48] A slight excess (10%) of the silane, 0.015 mmol, was added and the solution refluxed for 8 h. The mixture was filtered and washed successively with anhydrous solvents toluene, isopropyl alcohol, and acetone to remove unreacted silane. The solid product was dried overnight under a vacuum at room temperature. The schematic of the chemical structure synthesis is summarized in Scheme 1.

2.5. Fluorescence Studies for Metal Ion Detection. Each detection of metal ions was measured in a 0.01 M Tris-HCl buffer at pH 7.22. The stock solution of modified MCM-41 (**4**) was prepared in DIW (10.0 mg/2.0 mL). The concentration of **4** in the test solutions for fluorescence measurements was kept at a constant value of 100.0 μg/2.0 mL. Stock solutions of 0.1 M concentration of NaCl, KCl, $CaCl_2$, $MgCl_2$, $CrCl_2$, $MnCl_2$, $FeCl_2$, $CoCl_2$, $NiCl_2$, $CuSO_4 \cdot 5H_2O$, $ZnNO_3 \cdot 6H_2O$, $CdCl_2$, $HgCl_2$, $PbNO_3$, and $TlNO_3$ were prepared in DIW. Necessary dilutions were made according to each experimental setup. All fluorescence spectra were recorded at 22 °C with an excitation wavelength of 330 ± 5 nm.

2.6. Determination of Quantum Yield. Fluorescence quantum yields were determined at 22 °C with a slight modification of the procedure reported by Parker and Rees,[49] using quinine bisulfate in 0.1 M H_2SO_4 (Φ = 0.58) as the reference. For the metal-free study, 10 μL of 100 mM Na_4EDTA was added to a Tris-HCl buffer to chelate any adventitious metal ions, and a 10 mL suspension of 500 μg of **4** was prepared in the same buffer. The absorption of a standard reference was adjusted to the same value (Abs < 0.1, at excitation wavelength) as that of **4**. For the metal-bound studies, a 1 μM $ZnSO_4$ solution was prepared in a 10 mL suspension of 500 μg of **4**. The excitation wavelength was 330 ± 5 nm, and the emission intensities were obtained from integration between 400 and 650 nm. The quantum yields were calculated with eq 1.

$$\Phi_X = \Phi_{ST}\left(\frac{\mathrm{Grad}_X}{\mathrm{Grad}_{ST}}\right)\left(\frac{\eta_X^2}{\eta_{ST}^2}\right) \quad (1)$$

where the subscripts ST and X denote standard and test, respectively, Φ is the fluorescence quantum yield, Grad is the gradient from the plot of the integrated fluorescence intensity versus absorbance, and η is the refractive index of the solvent.

3. RESULTS AND DISCUSSION

3.1. Synthesis and Characterization of the Sensing Solid. In this study, we have designed a system on MCM-41 containing the 8-aminoquinoline group as a suitable chemosensor for the fluorescence sensing of zinc(II). The surface of MCM-41 was modified using molecular self-assembly of the organosilane **3**, as shown in Scheme 1, forming a new class of materials called self-assembled monolayers on mesoporous supports or SAMMS.[47,48] The performance of **4** was evaluated for the sensitivity and selectivity toward zinc(II) in aqueous media using fluorometric techniques.

The structural information of the fluorophore on the surface was studied by solid-state NMR and DRIFT spectroscopy. The ^{13}C NMR spectrum of the solid product **4** is plotted against the solution NMR of **3** in Figure SI1A (Supporting Information). The major resonances are labeled with the aromatic region between 122 and 142 ppm. Two resonances at 160 and 163 ppm correspond to the carbonyl group. This is attributed to the restricted motion of the organic moiety when fixed on the surface, causing different orientations of the ligand on the surface. The remaining resonances belong to the alkyl chain of the silane. The ethoxy groups (18 and 57 ppm of the silane in Figure SI1B in the Supporting Information) are not seen in the solid product, indicating complete hydrolysis of the groups before the self-assembly process takes over.[48]

The presence of the organic moiety as part of the silica wall structure of MCM-41 is confirmed by solid-state ^{29}Si MAS NMR

in Figure SI2 in the Supporting Information. The resonances at −57.48 and −67.31 ppm are the T^3 and T^4 sites, which represent the terminal and cross-linked siloxane groups, respectively, indicating the presence of a Si−C bond on the surface.[47,48,50] The major resonance at −110.28 ppm is the Q^4 site of the bulk silica (SiO_4 tetrahedron). The Q^2 and Q^3 sites, representing the geminal and vicinal hydroxyl groups, respectively, of unmodified MCM-41, are not easily discernible because they are converted to Q^4 sites upon binding of the silane.[51]

The DRIFT spectra of modified and unmodified MCM-41 are shown in Figure 1. In Figure 1A, the region 3400−3750 cm^{-1} represents the different silanols on the surface, with a narrow region of 3740−3746 cm^{-1} assigned to geminal and free hydroxyl groups.[52−54] Any adsorbed water on the surface is seen in the region 3400−3500 cm^{-1}, with the overtone structure vibrations attributed by the region 1750−1950 cm^{-1}. The band at 1629 cm^{-1} represents the bending mode of OH vibrations.[52,53] Compared to **4** (Figure 1B), the silanol bands disappear, while the NH vibration is seen at 3302 cm^{-1}. The typical range for aliphatic and aromatic CH stretches is observed around and above 2900 cm^{-1}, while the carbonyl (C═O) band is seen at 1686 cm^{-1}. The DRIFT spectra clearly indicate the presence of silane **3** on MCM-41.

Table 1 gives the results of elemental analysis, the BET specific surface area, the mean pore size diameter, and the total pore volume of unmodified and modified MCM-41. As expected, the BET surface area and pore size decrease upon grafting of the silane **3** on the MCM-41 surface. The CHN elemental analysis of **4** gives the C/N molar ratio as 4.8, which is almost the same as that of the organosilane **3** having released the three ethoxy groups, C/N = 4.66.[50] This is an indication that the functional group is grafted on the surface and did not decompose during the modification process.

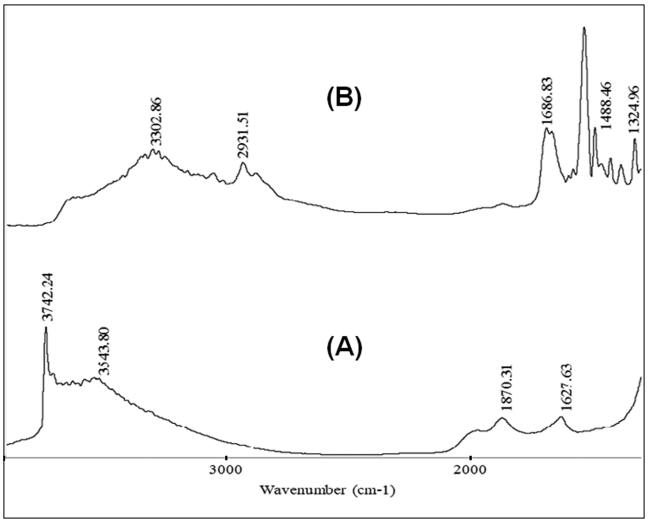

Figure 1. DRIFT spectrum showing the characteristic functional groups of (A) unmodified and (B) modified MCM-41 (**4**).

It should to be observed that functionalizing the surface does not affect the general morphology of MCM-41. TEM images of functionalized MCM-41 (Figure 2C,D) show that the hexagonal pore structure, along with longitudinal cylindrical channels, is retained after modification compared to unmodified MCM-41 (Figure 2A,B).

The TGA weight loss curves for modified and unmodified MCM-41 (Figure 3) provide a qualitative comparison of the changes induced after modification. The unmodified MCM-41 (Figure 3A) exhibits a weight loss at about 50 °C corresponding to the loss of physically adsorbed water, suggesting the surface to

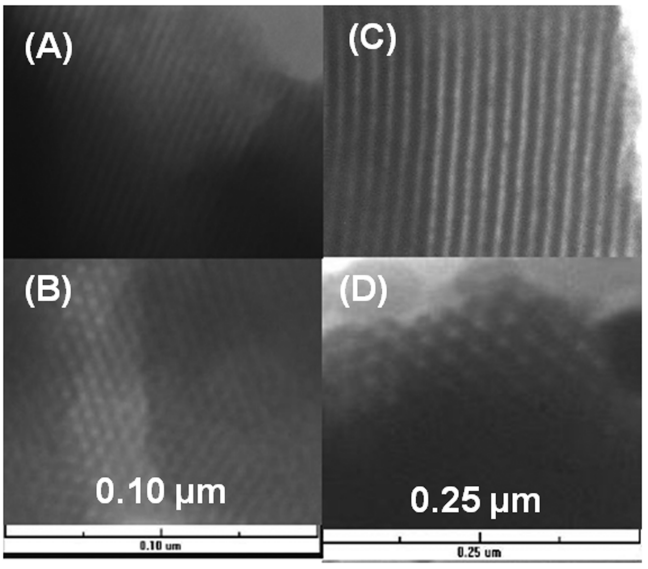

Figure 2. TEM images of (A and B) modified MCM-41 (**4**) and (C and D) unmodified MCM-41, where the scale bar is 0.25 and 0.10 μM, respectively.

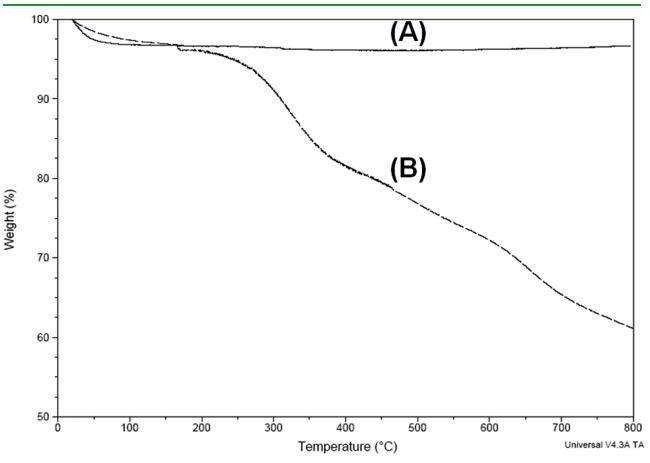

Figure 3. TGA weight loss curves of (A) unmodified and (B) modified MCM-41 (**4**).

Table 1. Structural Characteristics of Unmodified and Modified MCM-41 (4)

	S_{BET}[a] (m^2/g)	V_p[b] (mm^3/g)	D_p[c] (Å)	C (mmol/g)	N (mmol/g)	C/N molar ratio
unmodified MCM-41	880	1.3	37.0			
modified MCM-41 (**4**)	289	0.38	26.0	15.88	3.26	4.8

[a] BET specific surface area. [b] Primary mesoporous volume. [c] Pore diameter.

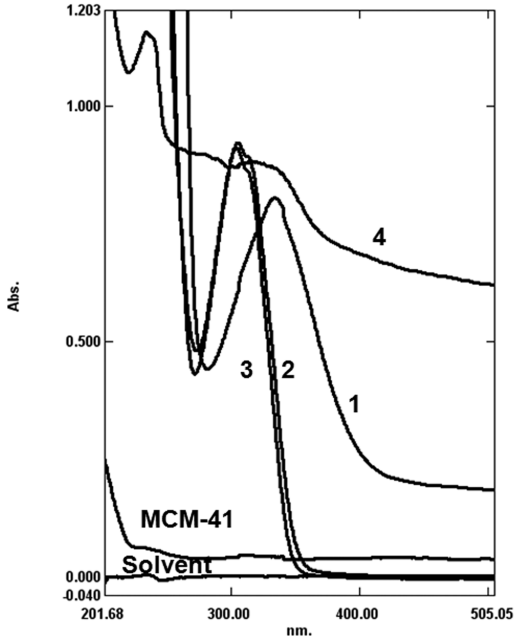

Figure 4. UV−vis absorption spectra of a Tris-HCl buffer, unmodified MCM-41, 8-aminoquinoline **1**, the chloroacetyl derivative of 8-aminoquinoline (**2**), silane **3**, and modified MCM-41 (**4**), showing absorption maxima between 295 and 360 nm.

be hydrophilic in nature.[55,56] With an increase in the temperature, the weight loss remains constant, indicating no appreciable condensation of silanol groups on the surface.[55,56] There is a significant change in the weight loss curve with modification of MCM-41 (Figure 3B). The resulting pattern in the weight loss curve depends on the nature of the ligand, and the step transition shows decomposition of the bonded organosilane, with the height being roughly proportional to the carbon content.[57]

In Figure 3B, three weight loss regions are seen: First, gradual weight loss up to 125 °C refers to the loss of any physically adsorbed water. This region is not as sharp as that observed in unmodified MCM-41, indicating a relative decrease in the hydrophilicity of the surface upon modification and an overall decrease in the surface silanol concentration.[55,56] Second, the weight loss between 150 and 375 °C is indicative of condensation of the ligand with any residual silanols on the surface and with silanols on neighboring ligands[58,59] represented by the T^2 sites in the ^{29}Si NMR spectrum in Figure SI2 in the Supporting Information. Third, gradual weight loss in the region 375−700 °C is due to decomposition of the organic ligand chemically bonded to the surface.[55]

Comparative UV−vis absorption spectra are shown in Figure 4. The absorption band of 8-aminoquinoline **1** appears at 330 nm, while those of the chloroacetyl derivative **2** and the silane **3** appear in the same region around 315 nm. The spectra of **4** show similar absorption bands from 320 to 340 nm, indicating that grafting of **3** on MCM-41 does not affect the inherent property of the fluorophore. The UV−vis spectra of unmodified MCM-41 and a Tris-HCl buffer (pH 7.22) do not show any bands in the fluorophore region and serve as negative control.

3.2. Zinc(II) Detection Studies. *3.2.1. Ligand Concentration on the Surface and Fluorescence Quantum Yield.* The concentration of the ligand molecules in a 100 μg/2 mL solution was calculated by the fluorescence method as described by Fang et al.[60] In this method, a calibration curve showing the relationship between the fluorescence intensity and the concentration of **2** in a solvent mixture of Tris-HCl and acetonitrile (Figure SI3 in the Supporting Information) is used to calculate the loading density of the ligand on the surface. The underlying assumption in using this method is that the quantum yield of the fluorophore is not affected by anchoring of the ligand on the surface and the fluorescence intensity of the fluorophore in low concentration is proportional to its concentration. Using the equation of a straight line (inset in Figure SI3 in the Supporting Information) and the intensity value of 1.01×10^6 corresponding to 100 μg of **4** in 2.0 mL solvent gives the fluorophore concentration as 29.3 ± 1.8 μM.

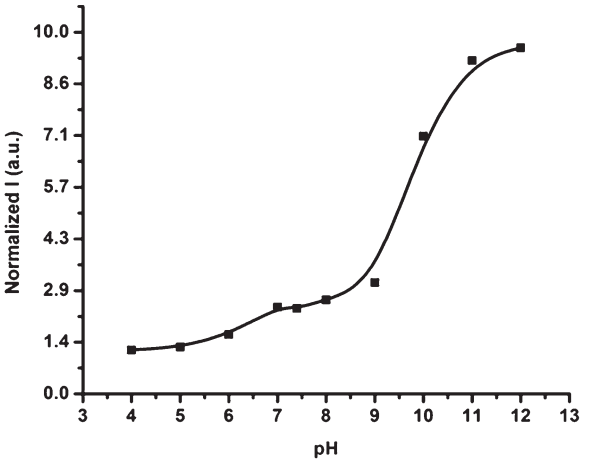

Figure 5. Fluorescence emission response of **4** (100 μg/2.0 mL) at different pH ranges, when treated with a 1.0 μM zinc(II) solution.

The fluorescence quantum yield of **4** was calculated to be 0.032 in a Tris-HCl buffer (pH 7.22), which was determined by using quinine bisulfate (0.1 M H_2SO_4; $\Phi = 0.58$) as the standard. The fluorescence emission intensity of **4** increases 3-fold with a red shift of 55 nm upon the addition of 1.0 μM zinc(II), and the quantum yield of the zinc(II) complex was calculated as 0.106. Within the ligand framework, the excited-state proton transfer in combination with intramolecular PET causes suppression of the fluorescence, resulting in a low quantum yield.[6,13,20,21] Zinc(II), however, can interrupt this excited-state proton transfer in 8-aminoquinoline and its derivatives, and through blocking of the PET process, a fluorescence enhancement is observed along with an increase in the quantum yield.[6] Zinc(II), versus other late transition metals, is not capable of one-electron redox activity and, having a filled d shell, cannot participate in electron- or energy-transfer mechanisms.[22]

3.2.2. pH Sensitivity of the Sensor and Time Titration. The performance characteristic of the sensor was tested for its sensitivity toward the pH. It is essential for the sensor to perform satisfactorily at physiological pH in order to apply it toward biological sensing. The response of the sensor toward zinc(II) at different pH values is reported in Figure 5. A 100.0 μg/2.0 mL stock solution of **4** containing a 1.0 μM zinc(II) solution is used for the experiment. In acidic environments, the response is low because of protonation of the amino group in the fluorophore, which, in turn, shows a low affinity toward zinc(II).[18] The fluorescence intensity, however, increases with an increase in the pH, and a small plateau was observed between pH 7.0 and 8.0, but the fluorescence emission intensity increases further in basic conditions up to pH 12. This increase could be attributed to

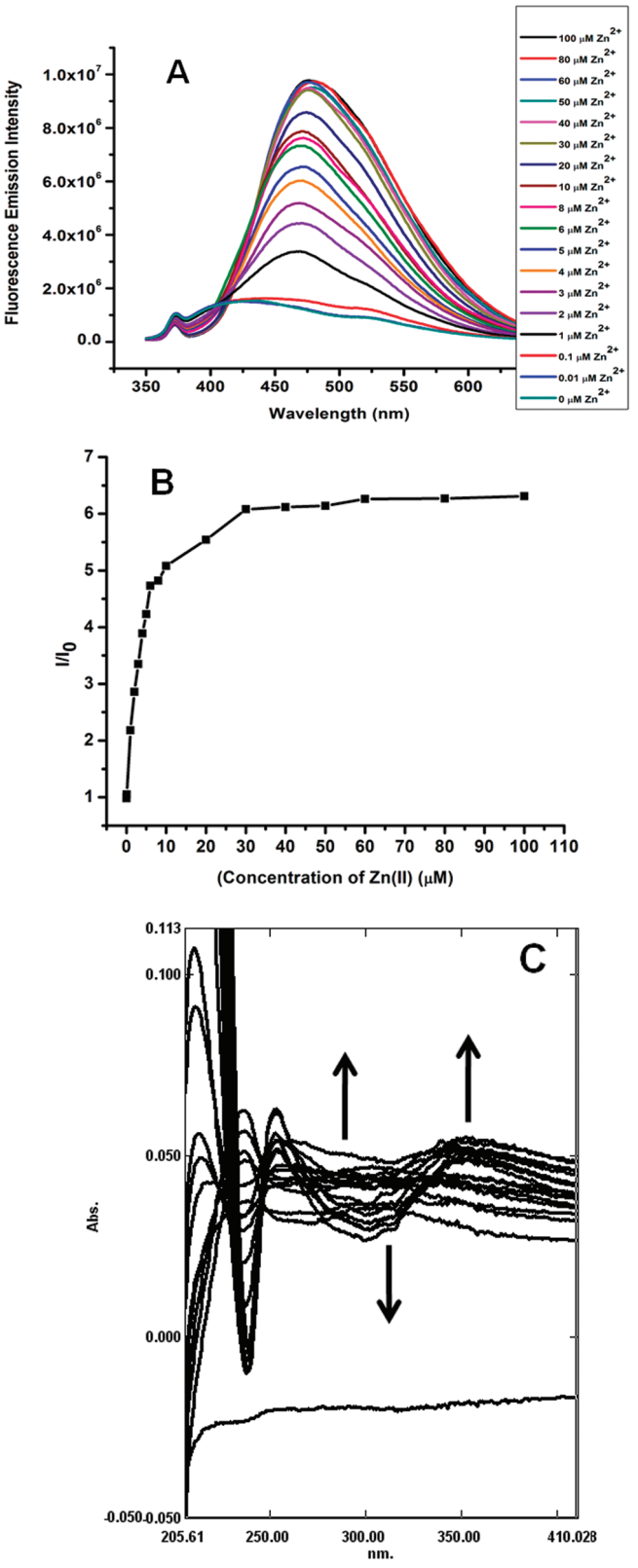

Figure 6. Fluorescence emission spectrum (A), titration curve (B), and UV−vis absorption spectrum (C) of **4** (100 μg/2.0 mL) in Tris-HCl (0.01 M, pH 7.22) in the presence of zinc(II) from 0.01 to 100 μM.

deprotonation of the amino group of the fluorophore, thereby increasing its affinity toward zinc(II). The pH study shows

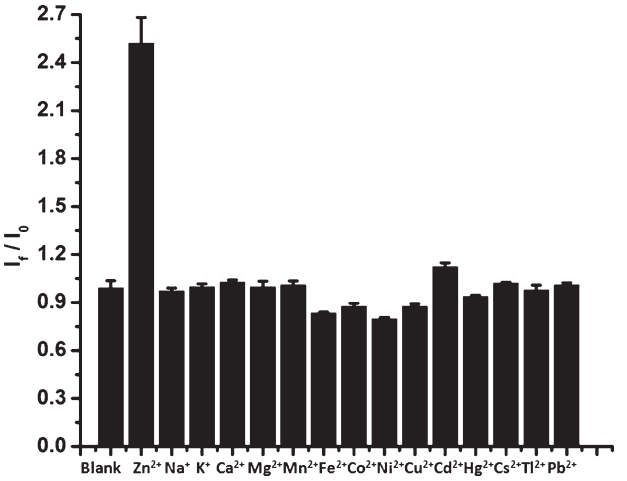

Figure 7. Bar graph of the fluorescence emission intensity for 15 different metals showing the metal selectivity profile of **4** (100 μg/2.0 mL) in Tris-HCl (0.01 M, pH 7.22) with a concentration of 1.0 μM for each metal.

(Figure 5) that use of the sensor is feasible under physiological pH.

In order to find the approximate time that equilibrium was established, a time titration experiment was performed. As shown in Figure SI4 in the Supporting Information, the fluorescence intensity increases from time zero to about 50 min and remains constant when equilibrium is established. The importance of this experiment is to establish a real-time use of the sensor within a short response time. For the remaining experiments, a reaction time of 50 min was set to ensure complete equilibration before measurement.

3.2.3. Sensor Detection Limit and Metal Studies. To determine the detection limit of the sensor toward zinc(II), the fluorescence emission was recorded under a very narrow concentration range from 0.01 to 100.0 μM (Figure 6A). There is a linear increase in the fluorescence intensity up to a zinc(II) concentration of 30 μM, and it remains fairly constant thereafter (Figure 6B). This result can be attributed to complex formation in a 1:1 mole ratio between the sensor and zinc(II). Moreover, a Job's plot,[61] which exhibits a maximum mole fraction of zinc(II) at approximately 0.5 M, further suggests the formation of a 1:1 complex (Figure SI5 in the Supporting Information). An association constant value of log K = 3.76 was obtained, which was calculated by a method developed by Martínez-Máñez et al.[62]

The UV−vis titration data of **4** with zinc(II) (0.01−100 μM concentration range) are shown in Figure 6C. A red shift of 45 nm from 310 to 355 nm is observed, with four isosbestic points at 233, 247, 272, and 332 nm, although in the red-shift region the last two isosbestic points are not easily distinguishable.

Spectrofluorometric titration of various metal ions (15) with the sensor **4** was performed to establish selectivity. The common biological elements such as sodium, potassium, calcium, magnesium, and iron, along with other first-row late-transition-metal ions, were used. In the first set of experiments, the fluorescence intensity was measured separately for the individual metal ions by using a 1.0 μM concentration of all metal ions. The maximum fluorescence intensities were plotted in a bar graph, as shown in Figure 7. This shows the selective response for zinc(II), while the other metal ions show no or little response. The corresponding fluorescence spectrum is shown in Figure SI6 in the Supporting

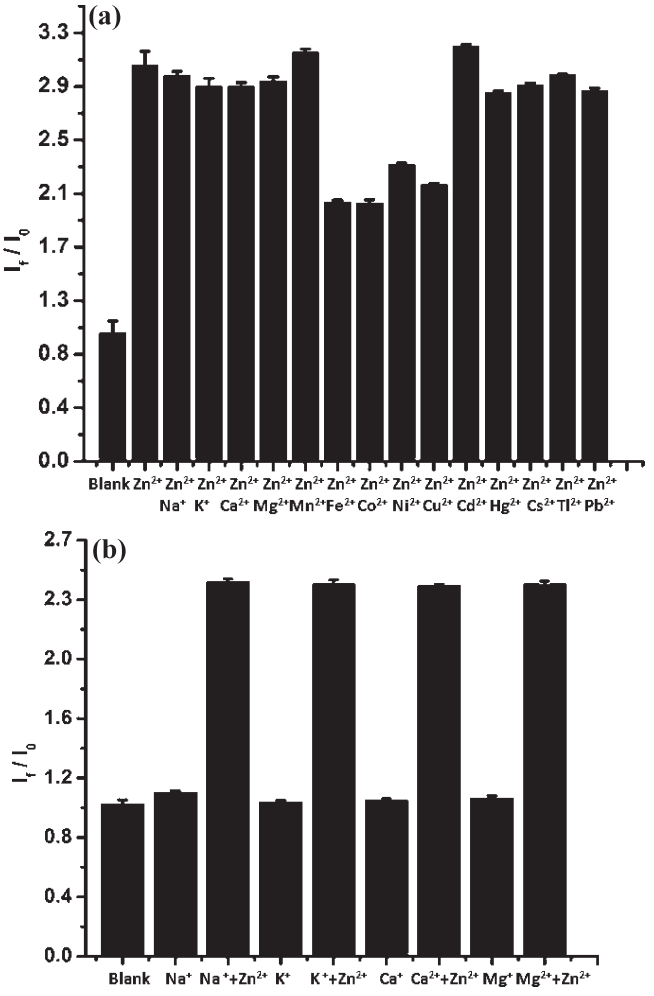

Figure 8. Relative fluorescence emission intensity of **4** (100 μg/2.0 mL) in Tris-HCl (0.01 M, pH 7.22) with metal ions in the presence of zinc(II), in an equimolar concentration of 1.0 μM (A). Relative fluorescence emission intensity of **4** (100 μg/2.0 mL) in Tris-HCl (0.01 M, pH 7.22) with zinc(II) at 1.0 μM and other metals at a higher concentration of 5.0 mM (B).

Information. The late transition metals, from iron to copper, exhibit a slight quenching of the fluorescence. These transition metals with partially filled 3d shells exhibit redox activity, and electron exchange is possible between the fluorophore and metal ions, resulting in the quenching of the fluorophore via nonradiative energy transfer.[13,22]

It is necessary, though, to study the competition of these metal ions in the presence of zinc(II). Additionally, some of these metal ions are present in a much higher concentration than zinc(II) in biological systems. Competition spectrofluorometric experiments with metal mixtures of zinc(II) with the other metal ions in equimolar concentrations (1.0 μM) were carried out as shown in Figure SI7 in the Supporting Information. The maximum intensities are plotted in a bar graph, as shown in Figure 8A. Although transition metals iron through copper compete with the binding sites, there is an overall increase in the fluorescence intensity with zinc(II) binding. It should also be noted that these metal ions, with the exception of iron(II), are present in low concentration or not present in vivo.

In another experiment, we kept the concentration of the common metal ions such as Na^+, K^+, Ca^{2+}, and Mg^{2+} at 5.0 mM while maintaining the concentration of Zn^{II} at 1.0 μM (Figure 8B). The higher concentration of the other metal ions does not affect the selectivity and sensitivity of the fluorophore toward zinc(II). This is clearly demonstrated from spectrofluorometric emission spectra as shown in Figure SI8 in the Supporting Information. Each experiment for the metal ion detection was performed in triplicate, and the value reported is the average with standard deviations (σ < 2−5%) presented in the bar graphs.

4. CONCLUSION

We have developed a new organic−inorganic, sensitive, and selective class of a zinc(II) fluorometric sensor using ordered mesoporous silica material, MCM-41, as a support and the 8-aminoquinoline derivative as the metal ion chelator and fluorescent moiety. The results of fluorescence experiments show a 3-fold zinc(II) enhancement in the emission intensities along with a red shift of 55 nm. The detection limit of 0.1 μM zinc(II) in a Tris-HCl buffer (pH 7.22) is observed. The presence of other metal ions does not affect the selectivity, even in the presence of high concentrations (5.0 mM) of Na^+, K^+, Ca^{2+}, and Mg^{2+} along with Zn^{II}. The above quinoline−MCM-41 sensor system is expected be used as a fluorescent material for the detection of zinc(II) in intercellular environments and water-quality monitoring.

■ ASSOCIATED CONTENT

Supporting Information. Solid-state ^{13}C NMR of **4**; solution ^{13}C NMR of silane **3**; solid-state ^{29}Si NMR of **4**; calibration curve of **2**; time titration line graph of **4** with zinc(II); Job's plot of **4** with zinc(II); fluorescence emission intensity spectra with 15 different metal ions; fluorescence emission intensity spectra with 15 different metal ions with zinc(II); fluorescence emission intensity spectra with in the presence of four different metal ions at high concentrations. This material is available free of charge via the Internet at http://pubs.acs.org.

■ AUTHOR INFORMATION

Corresponding Author

*Phone: +1-505-507-5681. Fax: +1-208-664-1272. E-mail: srastogi@uidaho.edu.

Author Contributions

‡These authors contributed equally toward this manuscript.

■ ACKNOWLEDGMENT

Financial support from the U.S. Department of Agriculture (Grant 2008-34479-19150) and the Center for Biological Applications of Nanotechnology (BANTech) group at the University of Idaho is gratefully acknowledged. The authors thank Franklin Bailey (electron microscopy center facility at the University of Idaho) for providing TEM images of MCM-41, Jeanne Shreeve, Department of Chemistry at the University of Idaho, for providing the elemental analyzer and TGA facility, and Alexander Blumenfeld for NMR.

■ REFERENCES

(1) Kimura, E.; Koike, T. *Chem. Soc. Rev.* **1998**, *27*, 179–184.
(2) You, Y.; Tomat, E.; Hwang, K.; Atanasijevic, T.; Nam, W.; Jasanoff, A. P.; Lippard, S. J. *Chem. Commun.* **2010**, *46*, 4139–4141.

(3) Nolan, E. M.; Lippard, S. J. *Acc. Chem. Res.* **2009**, *42*, 193–203.
(4) Domaille, D. W.; Que, E. L.; Chang, C. J. *Nat. Chem. Biol.* **2008**, *4*, 168–175.
(5) Fan, J.; Peng, X.; Wu, Y.; Lu, E.; Hou, J.; Zhang, H.; Zhang, R.; Fu, X. *J. Luminesc.* **2005**, *114*, 125–130.
(6) Jiang, P.; Guo, Z. *Coord. Chem. Rev.* **2004**, *248*, 205–229.
(7) Cotton, F. A.; Wilkinson, G. *Advanced Inorganic Chemistry*, 5th ed.; Wiley: New York, 1988.
(8) Chen, Y.; Han, K.-Y.; Liu, Y. *Bioorg. Med. Chem.* **2007**, *15*, 4537–4542.
(9) Qiu, L.; Jiang, P.; He, W.; Tu, C.; Lin, J.; Li, Y.; Gao, X.; Guo, Z. *Inorg. Chim. Acta* **2007**, *360*, 431–438.
(10) Nolan, E. M.; Burdette, S. C.; Harvey, J. H.; Hilderbrand, S. A.; Lippard, S. J. *Inorg. Chem.* **2004**, *43*, 2624–2635.
(11) Burdette, S. C.; Walkup, G. K.; Spingler, B.; Tsien, R. Y.; Lippard, S. J. *J. Am. Chem. Soc.* **2001**, *123*, 7831–7841.
(12) Bergonzi, R.; Fabbrizzi, L.; Licchelli, M.; Mangano, C. *Coord. Chem. Rev.* **1998**, *170*, 31–46.
(13) Valeur, B.; Leray, I. *Coord. Chem. Rev.* **2000**, *205*, 3–40.
(14) Prodi, L.; Bolletta, F.; Montalti, M.; Zaccheroni, N. *Coord. Chem. Rev.* **2000**, *205*, 59–83.
(15) Frederickson, C. J.; Kasarkis, E. J.; Ringo, D.; Frederickson, R. D. *J. Neurosci. Methods* **1987**, *20*, 91–103.
(16) Zalewski, P. D.; Forbes, I. J.; Betts, W. H. *Biochem. J.* **1993**, *296*, 403.
(17) Zalewski, P. D.; Forbes, I. J.; Seamark, R. F.; Borlinghaus, R.; Bette, W. H.; Lincoln, S. F.; Ward, A. D. *Chem. Biol.* **1994**, *3*, 153.
(18) Mahadevan, I. B.; Kimber, M. C.; Lincoln, S. F.; Tiekink, E. R. T.; Ward, A. D.; Betts, W. H.; Forbes, I. J.; Zalewski, P. D. *Aust. J. Chem.* **1996**, *49*, 561–568.
(19) Budde, T.; Minta, A.; white, J. A.; Kay, A. R. *Neuroscience* **1997**, *3*, 127–139.
(20) Van Meervelt, L.; Goethals, M.; Leroux, N.; Zeegers-Huyskens, Th. *J. Phys. Org. Chem.* **1997**, *10*, 680–686.
(21) Mu, L.; Shi, W.; Chang, J. C.; Lee, S.-T. *Nano Lett.* **2008**, *8*, 104–109.
(22) Fabbrizzi, L.; Licchelli, M.; Pallavicini, P.; Sacchi, D.; Taglietti, A. *Analyst* **1996**, *121*, 1763.
(23) Williams, J. N.; Reibenspies, J. H.; Hancock, R. D. *Inorg. Chem.* **2009**, *48*, 1407–1415 and references cited therein.
(24) Burdette, S. C.; Frederickson, C. J.; Bu, W.; Lippard, S. J. *J. Am. Chem. Soc.* **2003**, *125*, 1778–1787.
(25) Huston, M. H.; Haider, K. W.; Czarnik, A. W. *J. Am. Chem. Soc.* **1988**, *112*, 3590.
(26) Balzani, V.; Bolletta, F.; Gandolfi, M. T.; Maestri, M. *Top. Curr. Chem.* **1978**, *75*, 1–64.
(27) de Silva, A. P.; Gunaratne, H. Q. N.; Gunnlaugsson, T.; Huxley, A. J. H.; McCoy, C. P.; Rademacher, J. T.; Rice, T. E. *Chem. Rev.* **1997**, *97*, 1515–1566.
(28) de Silva, A. P.; Fox, D. B.; Huxley, A. J. H.; Moody, T. S. *Coord. Chem. Rev.* **2000**, *205*, 41–57.
(29) Callan, J. F.; de Silva, A. P.; Magri, D. C. *Tetrahedron* **2005**, *61*, 8551–8588.
(30) Liu, Y.; Zhang, N.; Chen, Y.; Wang, L. *Org. Lett.* **2007**, *9*, 315–318.
(31) Teolato, P.; Rampazzo, E.; Arduini, M.; Mancin, F.; Tecilla, P.; Tonellato, U. *Chem.—Eur. J.* **2007**, *13*, 2238–2245.
(32) Descalzo, A. B.; Rurack, K.; Weisshoff, H.; Martinez-Manez, R.; Marcos, M. D.; Amoros, P.; Hoffmann, K.; Soto, J. *J. Am. Chem. Soc.* **2005**, *127*, 184–200.
(33) Vartuli, J. C.; Schmitt, K. D.; Kresge, C. T.; Roth, W. J.; Leonowicz, M. E.; McCullen, S. B.; Hellring, S. D.; Beck, J. S.; Schlenker, J. L.; Olson, D. H.; Sheppard, E. W. *Chem. Mater.* **1994**, *6*, 2317.
(34) Koyano, K. A.; Tatsumi, T.; Tanaka, Y.; Nakata, S. *J. Phys. Chem. B* **1997**, *101*, 9436.
(35) Mercier, T.; Pinnavaia, T. J. *Adv. Mater.* **1997**, *9*, 500.
(36) Liu, J.; Feng, X.; Fryxell, G. E.; Wang, L. Q.; Kim, A. Y.; Gong, M. *Adv. Mater.* **1998**, *10*, 1.
(37) Beck., J. S.; Vartuli, J. C.; Roth, W. J.; Leonowicz, M. E.; Kresge, C. T.; Schmitt, K. D.; Chu, C. T. W.; Olson, D. H.; Sheppard, E. W.; McMcullen, S. B.; Higins, J. B.; Schlenker, J. L. *J. Am. Chem. Soc.* **1992**, *114*, 10834–10843.
(38) Kresge, C. T.; Leonowicz, M. E.; Roth, W. S.; Vartuli, J. C.; Beck, J. S. *Nature* **1992**, *359*, 710.
(39) Descalzo, A. B.; Jimenez, D.; El Haskouri, J.; Beltran, D.; Amoros, P.; Marcos, M. D.; Martinez-Manez, R.; Soto, J. *Chem. Commun.* **2002**, *6*, 562–563.
(40) Schulz-Ekloff, G.; Wohrle, D.; van Duffel, B.; Schoonheydt, R. A. *Microporous Mesoporous Mater.* **2002**, *51*, 91–138.
(41) Descalzo, A. B.; Jimenez, D.; Marcos, M. D.; Martinez-Manez, R.; Soto, J.; El Haskouri, J.; Guillem, C.; Beltran, D.; Amoros, P.; Borrachero, M. V. *Adv. Mater.* **2002**, *14*, 966–969.
(42) Descalzo, A. B.; Marcos, M. D.; Martinez-Manez, R.; Soto, J.; Bentran, D.; Amoros, P. *J. Mater. Chem.* **2005**, *15*, 2721–2731.
(43) Wark, M.; Rohlfing, Y.; Altindag, Y.; Wellmann, H. *Phys. Chem. Chem. Phys.* **2003**, *5*, 5188–5194.
(44) Brasola, E.; Mancin, F.; Rampazzo, E.; Tecilla, P.; Tonellato, U. *Chem. Commun.* **2003**, *24*, 3026–3027.
(45) Zhang, Y.; Guo, X.; Si, W.; Jia, L.; Qian, X. *Org. Lett.* **2008**, *10*, 473–476.
(46) Dong, Z.; Yang, B.; Jin, J.; Li, J.; Kang, H.; Zhong, X.; Li, R.; Ma, J. *Nanoscale Res. Lett.* **2009**, *4*, 335–340.
(47) Feng, X.; Fryxell, G. E.; Wang, L. Q.; Kin, A. Y.; Lu, J.; Kemner, K. M. *Science* **1997**, *276*, 923–926.
(48) Fryxell, G. E.; Mattigod, S. V.; Lin, Y.; Wu, H.; Fiskum, S.; Parker, K.; Zheng, F.; Yantasse, W.; Zemanian, T. S.; Addelman, R. S.; Liu, J.; Kemner, K.; Kelly, S.; Feng, X. *J. Mater. Chem.* **2007**, *17*, 2863–2874.
(49) Parker, C. A.; Rees, W. T. *Analyst* **1960**, *85*, 587–600.
(50) Yokoi, T.; Tatsumi, T.; Yoshitake, H. *J. Colloid Interface Sci.* **2004**, *274*, 451–457.
(51) Zhao, X. S.; Lu, G. Q.; Whittaker, A. K.; Millar, G. J.; Zhu, H. Y. *J. Phys. Chem. B* **1997**, *101*, 6525–6531 and references cited therein.
(52) Vrancken, K. C.; Van der Voort, P.; Gillis-D'Hamers, I.; Vansant, E. F.; Grobet, P. *J. Chem. Soc., Faraday Trans.* **1992**, *88*, 3197–3200.
(53) Murthy, R. S. S.; Leyden, D. E. *Anal. Chem.* **1986**, *58*, 1228–1233.
(54) Chiang, C.; Liu, N.; Koenig, J. L. *J. Colloid Interface Sci.* **1982**, *86*, 26–30.
(55) Jaroniec, C. P.; Gilpin, R. K.; Jaroniec, M. J. *J. Phys. Chem. B* **1997**, *101*, 6861–6866.
(56) Iler, R. K. *The Chemistry of Silica: Solubility, Polymerization, Colloid and Surface Properties, and Biochemistry*; Wiley: New York, 1979.
(57) Jaroniec, C. P.; Kruk, M.; Jaroniec, M.; Sayari, A. *J. Phys. Chem. B* **1998**, *102*, 5503–5510.
(58) Scott, R. P. W. *Silica Gel and Bonded Phases*; John Wiley & Sons: Chichester, U.K., 1993.
(59) Vansant, E. F.; Van der Voort, P.; Vrancken, K. C. *Characterization and Modification of the Silica Surface*; Elsevier: Amsterdam, The Netherlands, 1995.
(60) Lu, F.; Gao, L.; Li, H.; Ding, L.; Fang, Y. *Appl. Surf. Sci.* **2007**, *253*, 4123–4131.
(61) Zachary, D. H.; Patrick, M. C. *J. Chem. Educ.* **1986**, *68*, 163–167.
(62) Descalzo, A. B.; Marcos, M. D.; Martínez-Máñez, R.; Soto, J.; Beltrán, D.; Amorós, P. *J. Mater. Chem.* **2005**, *15*, 2721–2731.